ChemPhysChem

Research Article
doi.org/10.1002/cphc.202300848

Chemistry Europe
European Chemical Societies Publishing

www.chemphyschem.org

Liquid Crystal Dimers and the Twist-Bend Phases: Non-Symmetric Dimers Consisting of Mesogenic Units of Differing Lengths

Calum J. Gibb,*[a] Magdalena Majewska,[b] Damian Pociecha,[b] John M.D. Storey,[a] Ewa Gorecka,[b] and Corrie T. Imrie[a]

The syntheses and characterisation of the 4-[{[4-({*n*-[4-(4-cyanophenyl)phenyl]-*n*-yl}oxy)phenyl]-methylidene}amino]phenyl-4-alkoxybenzoates (CB*n*OIBeO*m*) are reported with $n = 8$ and 10 and $m = 1$–10. The two series display fascinating liquid crystal polymorphism. All twenty reported homologues display an enantiotropic nematic (N) phase at high temperature. When the length of the spacer (*n*) is greater than that of the terminal chain (*m*), the twist-bend nematic (N_{TB}) phase is observed at temperatures below the N phase. As the length of the terminal chain is increased and extends beyond the length of the spacer up to three smectic phases are observed on cooling the N phase. One of these smectic phases has been assigned as the rare twist-bend smectic C subphase, the $SmC_{TB\text{-}\alpha}$ phase. In all the smectic phases, a monolayer packing arrangement is seen, and this is attributed to the anti-parallel associations of the like mesogenic units.

Introduction

In recent years the twist-bend nematic (N_{TB}) phase has been the focus of considerable research due to its fascinating chiral properties despite being comprised of molecules which are themselves achiral.[1–6] In the N_{TB} phase the director spontaneously adopts a heliconical structure in which it is tilted with respect to the helical axis. The formation of chirality is spontaneous and equal numbers of left and right-handed helices are formed. This double degeneracy may be removed by molecular chirality and the chiral N_{TB} phase is formed.[7,8] With an ever-expanding library of twist-bend nematogens being reported (for example[9–13]) it is surprising how little is still understood about the relationship between molecular structure and the formation of the N_{TB} phase besides the requirement for the molecules to have an overall bent-molecular shape. This structural prerequisite was predicted independently by both Meyer[14] and Dozov.[15]

In his prediction of the N_{TB} phase,[15] Dozov also postulated the possibility of a heliconical twist-bend smectic (SmC_{TB}) phase which, like the N_{TB} phase, should be formed from bent achiral molecules. The existence of the SmC_{TB} was experimentally discovered for achiral bent liquid crystal dimers in 2018.[16,17] In the SmC_{TB} phase, the director is tilted with respect to the layer normal, and the tilt direction describes a helix on passing between layers. Little is known with regards to the molecular factors that drive the formation of SmC_{TB} phases. Trends in behaviour are beginning to emerge however with regards to the tendency to exhibit the singly and doubly helical variants of the SmC_{TB} phase, referred to as the $SmC_{TB\text{-}SH}$ and $SmC_{TB\text{-}DH}$, respectively. These phases have been observed only in dimers containing cyanobiphenyl and benzylideneaniline mesogenic units connected by an odd-membered spacer possessing a long terminal chain.[18–21]

The $SmC_{TB\text{-}\alpha}$ phase was the first heliconical twist-bend smectic phase to be discovered and found for the non-symmetric liquid crystal dimers the CB6OIBeO*m* series (Figure 1; $n = 6$).[22] Despite being the first SmC_{TB} phase observed, it remains the rarest. The CB6OIBeO*m* series shows a fascinating and rich phase behaviour. When the terminal chain (*m*) is shorter than the central spacer (*n*), i.e. $n > m$, conventional nematic (N) and N_{TB} phases are observed. The conventional N phase is shown for all terminal chain lengths, whereas, the N_{TB} phase is extinguished at $m = 7$. For $m \geq 7$, up to four smectic phases are observed. On decreasing temperature, these are the smectic A (SmA), biaxial smectic A (SmA_b) and a soft-crystalline hexatic-type smectic phase (HexI), and, when $m = 7$ and 8, the $SmC_{TB\text{-}\alpha}$ phase is also observed. Regardless of the length of the terminal chain, all the liquid-like smectic phases have periodicities comparable to the full molecular length (i.e. a *monolayer* structure). This is a departure from the behaviour of other non-symmetric dimers for which an evolution from intercalated to interdigitated arrangements is seen on increasing *m* depending on the length of the spacer (see, for example,[23–25]). This change in structure is often attributed to

[a] C. J. Gibb, J. M.D. Storey, C. T. Imrie
Department of Chemistry,
School of Natural and Computing Sciences,
University of Aberdeen,
Meston Building, Aberdeen AB24 3UE (UK)
E-mail: c.j.gibb@leeds.ac.uk

[b] M. Majewska, D. Pociecha, E. Gorecka
University of Warsaw,
Faculty of Chemistry,
ul. Zwirki i Wigury 101, 02-089 Warsaw, Poland

Supporting information for this article is available on the WWW under https://doi.org/10.1002/cphc.202300848

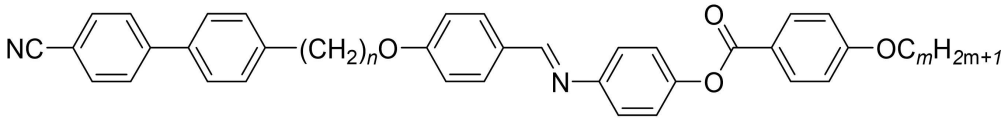

Figure 1. The general structure of the CB*n*OIBeO*m* series where $n = 8$ and 10, $m = 1$-10.

the ability of the terminal chain to be accommodated within the volume of the intercalated structure determined by the spacer.[26–28] The phase behaviour of the CB6OIBeO*m* dimers appears to be intrinsically linked to the *n*:*m* ratio with the $SmC_{TB-\alpha}$ phase only appearing when $n \approx m$. Further investigations of dimers containing structurally similar mesogenic units are now required in order to better understand these intriguing twist-bend phases and to establish the structure-property relationships regarding their formation.

Herein we report the synthesis and characterisation of the 4-[{[4-({*n*-[4-(4 cyanophenyl)phenyl]*n*-yl}oxy)phenyl]-methylidene}amino]phenyl-4-alkoxybenzoates (CB*n*OIBeO*m*) (Figure 1) with $n = 8$ and 10, $m = 1$–10. The properties of these dimers are compared to those of the CB6OIBeO*m* series[22] and allow the effect of increasing spacer length to be established.

Experimental

Synthesis

The synthetic route used to obtain the CB*n*OIBeO*m* series is shown in Scheme 1. The method is based on synthetic procedures described elsewhere.[25] Complete synthetic details, structural and purity analysis for final products and their intermediate compounds are provided in the ESI.

Results and Discussion

Extending the length of the spacer from $n = 6$ in the CB6OIBeO*m* series[22] to 8 and 10 in the CB8OIBeO*m* and CB10OIBeO*m* series, respectively, does not change the phase sequence observed but rather sees a shift in like transitions to longer terminal chain lengths reflecting the importance of the *n*:*m* ratio in determining phase behaviour. The temperature dependence of the transition temperatures for the CB8OIBeO*m* and CB10OIBeO*m* series on the length of the terminal chain, *m*, is shown in Figure 2 [above] and [below], respectively, and the accompanying transitional data are provided in the ESI (SITable 1 and SITable 2, respectively). All members of both series display an enantiotropic conventional nematic (N) phase which is assigned using polarized light optical microscopy (POM) by the observation of a characteristic schlieren texture containing 2 and 4-point brush singularities between untreated glass slides and which flashes when mechanical stress is applied. A uniform texture is observed when the samples are viewed within cells treated for planar alignment and unidirectionally rubbed. When the length of the terminal chain is shorter than that of the spacer ($n > m$), the N_{TB} phase is observed on cooling the conventional N phase. The N_{TB} phases were assigned using POM by the appearance of either rope-like or blocky textures when viewed between untreated glass slides and by a striped texture when viewed within a thin cell treated for planar alignment (for example see Figure 3 and SIFigure 1). The observation of this striped texture is now thought to be characteristic of the N_{TB} phase. It was attributed to undulation of the helical axis parallel to the surfaces (horizontal chevron) but also perpendicular to the surfaces (vertical chevron) that leads to a spatial variation of the optic axis direction and, in turn, to the appearance of a stripe pattern in optical textures observed under a polarizing microscope.[29,30] The values of T_{NTB-N} shown in Figure 2 were measured using POM and these transitions were not evident using DSC. This presumably reflects the weakly first order or continuous nature of the N-N_{TB} phase transition given the large temperature range of the preceding nematic phase.[1] The temperature dependence of the optical birefringence (Δn) is also consistent with the assignment of the N_{TB} phase with a characteristic decrease observed at the N-N_{TB} transition due to the averaging of optical anisotropy associated

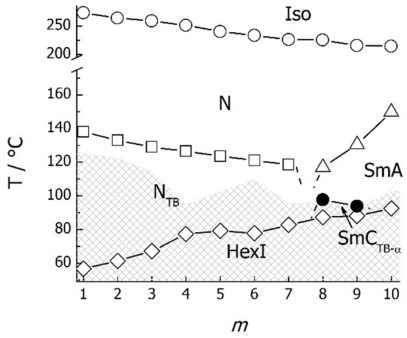

2) [29,31].

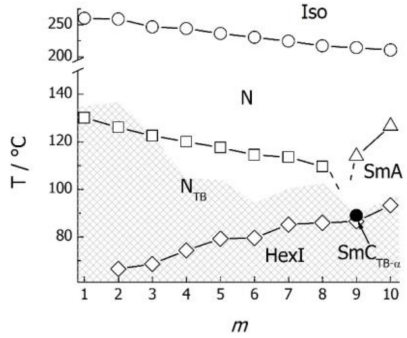

Figure 2. Phase diagrams for the CB8OIBeO*m* [above] and CB10OIBeO*m* [below] series. The crossed areas indicate monotropic regions.

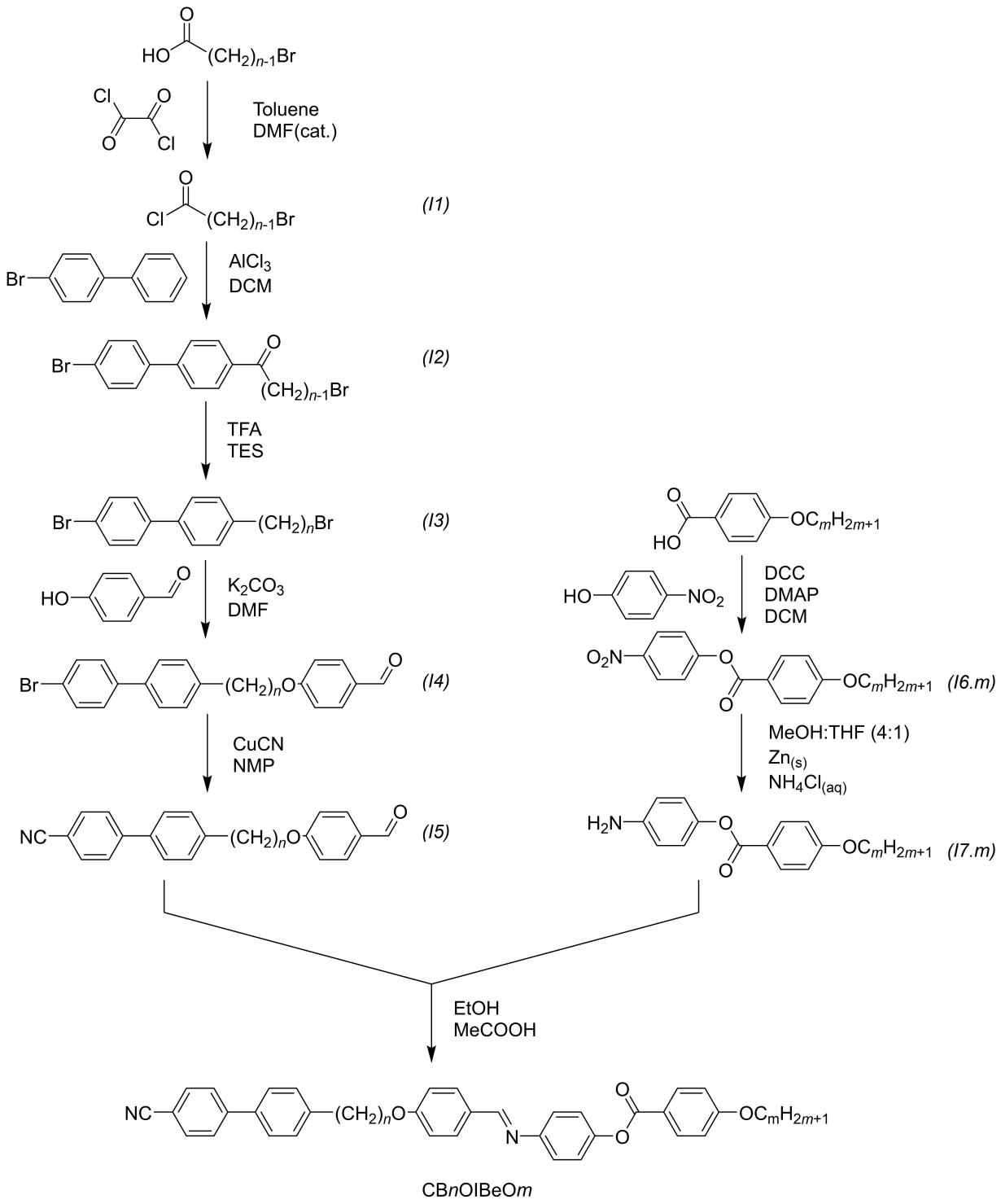

Scheme 1. The synthesis of the CB*n*OIBeO*m* series, where $n = 8$ and 10 and $m = 1$–10.

with the formation of the short-pitched helix (see SIFigure 2).[29,31]

The dependence of the N–I and N_{TB}-N transition temperatures on increasing *m* for the series with the longer spacers is essentially the same as seen for the CB6OIBeO*m* series, and specifically, increasing *m* sees a linear decrease in the values of $T_{N\text{-}I}$ and $T_{NTB\text{-}N}$. For the N–I transition, this reflects the dilution of the interactions between the mesogenic units due to the increased volume fraction of alkyl chains.[32] The decrease in the values of $T_{NTB\text{-}N}$ on increasing *m* is weaker than that seen for the values of $T_{N\text{-}I}$, and reflects the predominantly shape driven nature of the N_{TB}-N phase transition.[1,3,25]

The lowest temperature phase exhibited by all members of the series when $n = 8$ and, for $m > 2$ when $n = 10$ was assigned

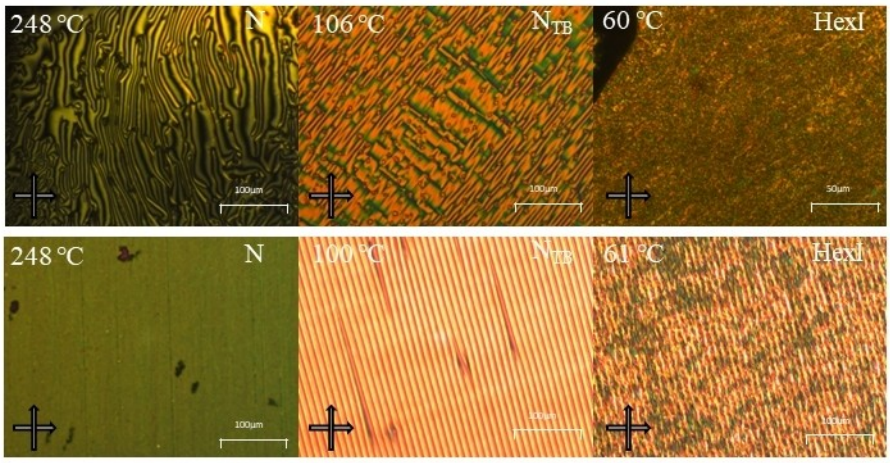

Figure 3. POM textures viewed between untreated glass slides (top) and within a 1.6 μm cell treated for planar alignment (bottom) of the N, N_{TB} and HexI phases observed for CB10OIBeO2.

as the tilted lamellar HexI phase. The identification of the HexI phase using POM is non-trivial as the textures are paramorphotic, however, X-ray diffraction studies clearly showed narrowing of the high-angle diffraction signal (SIFigure 3) evidencing increased correlations of molecular positions within the layers, characteristic for hexatic phases. AFM images (Figure 4) showed that although the structure of the HexI phase is lamellar, its morphology is sponge-like, and composed of interconnected empty channels with thin walls made of mesogenic material, the characteristic size being 100–200 nm. The scaled entropy changes associated with the HexI transitions are lower than those expected for crystallisation and appear as first-order transitions by DSC with little hysteresis on repeated heating and cooling cycles.

On increasing the terminal chain length ($n < m$), the N_{TB} phase is extinguished and replaced by up to two liquid-like smectic phases. The higher temperature smectic phase has been assigned as the SmA phase. Between untreated glass slides, the SmA phase is observed as either focal conic fans or the samples align homeotropically and a uniformly dark texture is seen (see Figure 5). In an aligned cell treated for a planar alignment, the SmA phase has a uniform texture like that of the

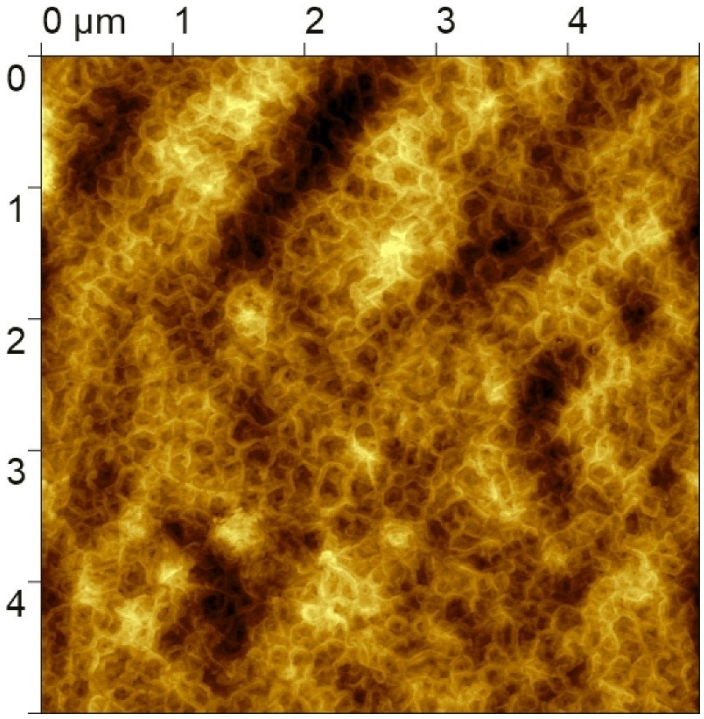

Figure 4. AFM image of CB6OIBeO7 in the HexI phase; the material was placed on silica substrate and quickly cooled to room temperature.

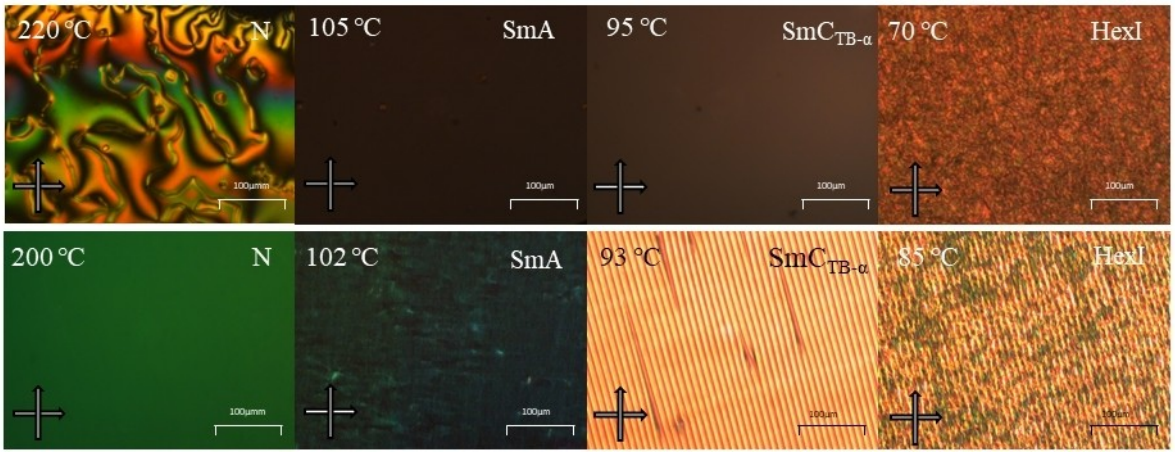

Figure 5. POM textures viewed between untreated glass slides (top) and within 1.6 μm cell treated for planar alignment (bottom) for the N, SmA, SmC$_{TB-\alpha}$ and HexI phases observed for CB8OIBeO8.

nematic phase, however, with increased optical birefringence (Figure 6c). Moreover, a distinct first-order transition is observed at the SmA–N transition in the DSC thermograms (see Figure 6a). The temperature dependence of the layer spacing (*d*) is also consistent with a SmA phase, with *d* increasing essentially linearly on cooling (see Figure 6b). The layer spacing corresponds approximately to the molecular length ($d \approx L$) indicating a monolayer structure as also observed for the CB6OIBeO*m* series.[22] For a given spacer length, increasing *m* sees a steep increase in the SmA–N transition temperature which is consistent with the view that increasing molecular inhomogeneity drives microphase separation and the formation of the SmA phase.

When the length of the terminal chain is approximately equal to the length of the spacer ($n \approx m$) (for $n = 8$, $m = 8\&9$, and for $n = 10$, $m = 9$), a further liquid-like smectic phase is observed at temperatures below the SmA phase. A very small enthalpy change is detected at the transition in the DSC thermogram (see Figure 6a) and the temperature dependence of the layer spacing indicates a transition to a tilted 'SmC-like' phase, the periodicity of which corresponds to about the molecular length (see Figure 6b). When viewed using POM between untreated glass slides, the low temperature phase cannot be distinguished from the SmA phase given both adopt homeotropic textures, but a wavefront can be observed that indicates the transition between the two phases. This precludes the assignment of conventional SmC$_s$ or SmC$_a$ phases as these are optically biaxial phases. When confined in a cell treated for planar alignment, the phase transition is well-defined, and the lower temperature phase shows a striped texture (see Figure 5). As described earlier for the N$_{TB}$ phase, the observation of a striped texture is characteristic for materials in which helical pitch varies with temperature, such temperature variation leads to the some helix axis undulations in cells.[18,22,31] The temperature dependence of the optical birefringence is also consistent with this assignment of an SmC$_{TB}$ phase, as a continuous decrease in Δn is seen throughout the phase (see Figure 6c and SIFigure 5). This is thought to arise from increasing tilt in the heliconical structure of the SmC$_{TB}$ phase. The optical uniaxiality of the SmC$_{TB}$ phase observed here precludes the assignment of

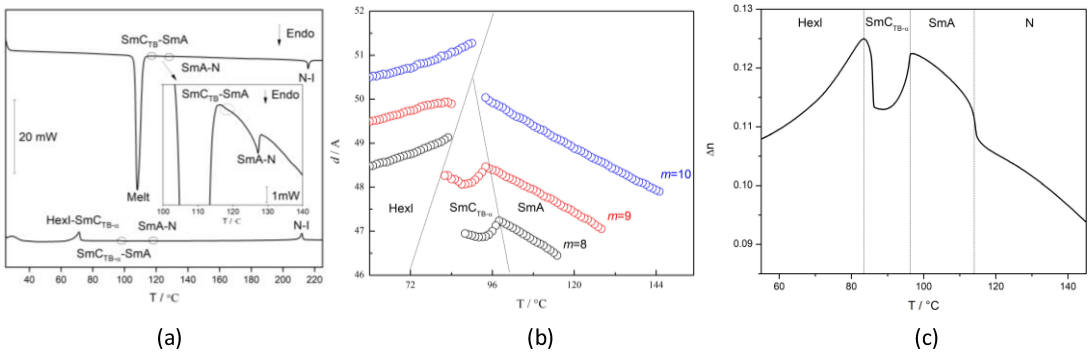

Figure 6. (a) DSC thermogram for CB8OIBeO8 showing the N-SmA-SmC$_{TB-\alpha}$-HexI phase sequence. (b) Smectic layer spacing (*d*) vs temperature for the CB8OIBeO*m* series with $m = 8$–10. For $m = 8$ and 9, the temperature dependence of the layer spacing, T(*d*), suggests a transition from an orthogonal SmA to a tilted smectic phase. (c) The temperature dependence of the optical birefringence, T(Δn), for CB8OIBeO8 measured in a 1.7 μm cell treated for planar alignment. Similar temperature dependencies of *d* and Δn shown in (b) and (c), respectively, have been observed previously for the SmC$_{TB-\alpha}$ phase for the CB6IBeO*m* series.[22]

the $SmC_{TB\text{-}SH}$ phase, in which the single distorted helix gives rise to optically biaxiality.[18] The second helical modulation present in the $SmC_{TB\text{-}DH}$ phase leads to the phase appearing optically uniaxial, but this has only been observed so far only for smectic phases with a bilayer structure.[18–20,24] This strongly suggests that the variant of the SmC_{TB} phase observed for the two series reported here is the $SmC_{TB\text{-}\alpha}$ phase and this is in accord with the assignment made previously for the CB6OIBeO*m* series.[22]

Let us now turn our attention to a comparison of the CB*n*OIBeO*m* series.[22] Increasing the length of the spacer sees a decrease in the values of $T_{N\text{-}I}$, $T_{NTB\text{-}N}$ and $T_{SmA\text{-}N}$ for a given terminal chain length (see Figure 7). For the values of $T_{N\text{-}I}$, this reflects an increase in molecular flexibility on increasing *n*, and a dilution of the interactions between the mesogenic units. As mentioned previously, the formation of the N_{TB} phase is thought to be predominantly shape driven[25] and the decrease in the values of $T_{NTB\text{-}N}$ reflects to a large extent the decrease in molecular curvature on increasing spacer length, *n*. The decrease in the values of $T_{SmA\text{-}N}$ may again reflect, at least in part, the dilution of intermolecular interactions due to the increased volume fraction of alkyl chains. In addition, the molecular inhomogeneity arising from a given terminal chain is greater for the shorter spacers and drives the formation of the smectic phase.

The layer spacing in the smectic phases shown by all three CB*n*OIBeO*m* series correspond to about the molecular length, irrespective of the *n*:*m* ratio. As we noted earlier, previous studies of non-symmetric dimers based on cyanobiphenyl and benzylideneaniline moieties showed that increasing the length of the terminal chain results in an evolution of the local structure within the smectic phases. Specifically, when the length of the spacer is greater than that of the terminal chain ($n > m$), an intercalated arrangement of the molecules is often observed.[26,28] This intercalated arrangement is thought to be driven by favourable quadrupolar interactions between the dissimilar cyanobiphenyl and benzylideneaniline mesogenic cores and additionally the terminal chains may be packed alongside the spacer. For longer chains, an interdigitated structure forms driven by antiparallel associations between the cyanobiphenyl units.[27] Between these two regimes only nematic behaviour is usually observed. The behaviour of the three CB*n*OIBeO*m* series is clearly quite different and strongly suggests that the driving force for the smectic phase formation must differ.

In order to better understand this differing behaviour, we first compare the structures of the CB*n*OIBeO*m* series reported here to the smaller, cyanobiphenyl-benzylideneaniline-based materials, the CB*n*O.O*m* series,[25] reported previously. In the case of the CB*n*O.O*m* series, the differing mesogenic units are of a similar size and there is electronic conjugation across the benzylideneaniline-based mesogenic unit with a single area of enhanced electron density focused on the nitrogen of the Schiff-base linking group (see Figure 8a). It is thought that the quadrupole moment arising from these electron rich and deficient areas interact with quadrupole moments of opposite signs on the cyanobiphenyl fragments driving the intercalated packing.[26,37,38] In the CB*n*OIBeO*m* series, the larger benzylideneaniline benzoate-based mesogenic unit is much larger than the cyanobiphenyl moiety. Electronic conjugation is possible across the imine-linking group but the ester bond acts effectively as a break giving two distinct regions of enhanced electron density (Figure 8b). The second localised area of electron density associated with the benzoate moiety prohibits the intercalation of the cyanobiphenyl and benzylideneaniline benzoate units as this would lead to unfavourable interactions between quadrupoles of the same sign. Instead, a more likely structure is based upon favourable interactions between neighbouring benzylideneaniline benzoate moieties with the two regions of localised electron density at either side of the ester-linkage driving the molecules into an anti-parallel arrangement (Figure 9). Such an arrangement would be further stabilised by the anti-parallel association of the cyanobiphenyl units at the layer interfaces and is consistent with the almost monolayer periodicity observed by X-ray diffraction.

Conclusions

The synthesis and characterisation of the CB*n*OIBeO*m* series with $n = 8$ and 10 ($m = 1$–10) has been reported. Their transitional behaviour is similar to that observed for the CB6OIBeO*m* series reported previously.[22] Increasing the length of the spacer sees a shift of like phase transitions to higher values of *m* and the associated transition temperatures decrease. This highlights that the phase behaviour observed is dependent on the ratio

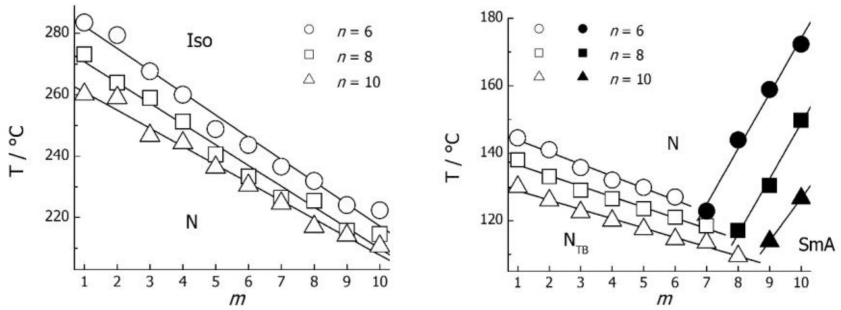

Figure 7. Comparison of the $T_{N\text{-}I}$ [left] and $T_{NTB\text{-}N}$ (open symbols) & $T_{SmA\text{-}N}$ (solid symbols) [right] for the three CB*n*OIBeO*m* series with $n = 6$ [circles] 8 [squares] and 10 [triangles].

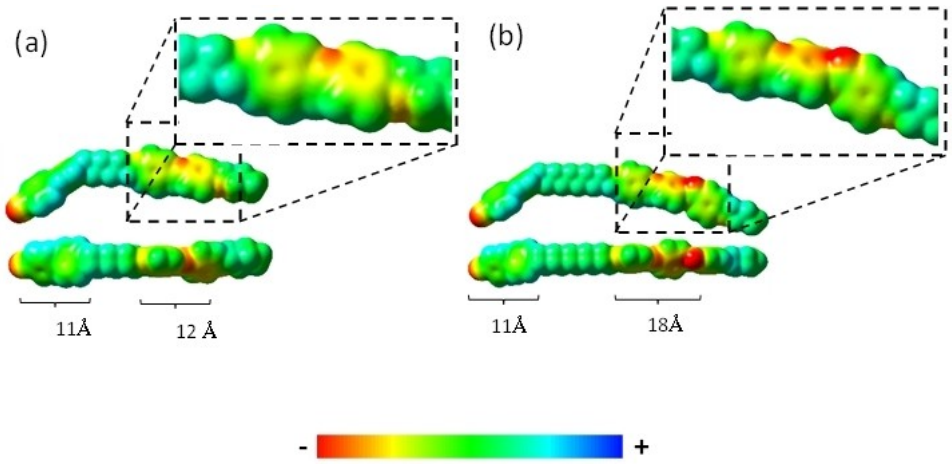

Figure 8. Electrostatic surface potential mapped as a function of total electron density for (a) CB6O.O4 and (b) CB10OIBeO4.[33–36] In the larger benzylideneaniline benzoate-based dimer, the two regions of enhanced electron density are clearly visible.

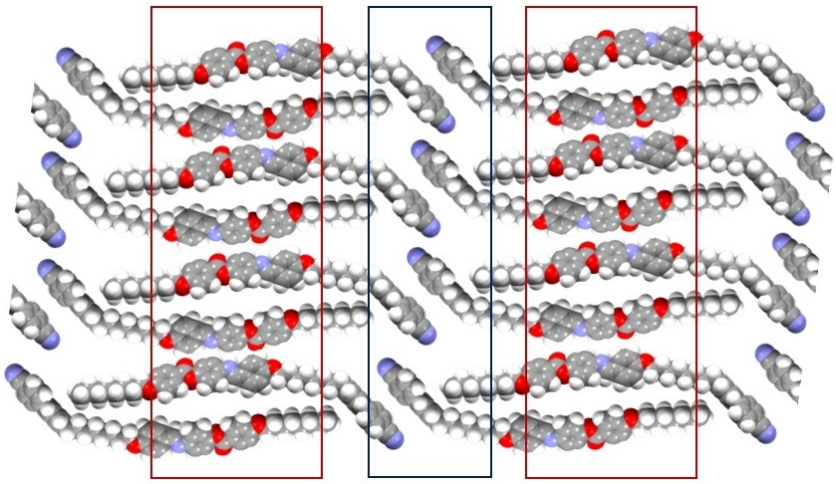

Figure 9. A schematic representation showing the proposed intermolecular interactions between molecules of CB8OIBeO8. The boxes indicate the antiparallel associations between the (red) benzilidineaniline benzoate mesogenic units and the (blue) cyanobiphenyl mesogenic units.

between the length of the terminal chain to the length of the spacer (n:m). When $n > m$, the N_{TB} phase is observed at temperatures below the conventional N phase. The emergence of smectic phases is seen when $n \approx m$, and we report three examples of the rare $SmC_{TB\text{-}\alpha}$ phase for CB8OIBeO8, CB8OIBeO9, and CB10OIBeO9. For $m > n$, the SmC_{TB} phase is extinguished and the SmA phase is the only liquid-like smectic phase observed. In all these phases, a monolayer packing arrangement is seen, and this is attributed to the anti-parallel association of the benzylideneaniline benzoate mesogenic units. Such an arrangement is further stabilised by the anti-parallel association of the cyanobiphenyl units.

Conflict of Interests

The authors declare no conflict of interest.

Data Availability Statement

The data that support the findings of this study are available from the corresponding author upon reasonable request.

Keywords: Liquid Crystals · Material Science · Mesophases · Monolayers · Twist-bend nematic phase · Twist-bend smectic phase

[1] D. A. Paterson, M. Gao, Y. K. Kim, *Soft Matter.* **2016**, *12*(32), 6827–6840.
[2] D. A. Paterson, *Soft Matter* **2016**, *12*, 6827.
[3] M. Cestari, E. Frezza, A. Ferrarini, G. R. Luckhurst, *J. Mater. Chem.* **2011**, *21*, 12303.
[4] P. A. Henderson, C. T. Imrie, *Liq. Cryst.* **2011**, *38*, 1407.
[5] V. Borshch, Y. K. Kim, J. Xiang, *Nat. Commun.* **2013**, *4*, 2635.
[6] D. Chen, J. H. Porada, J. B. Hooper, *Proc. Natl. Acad. Sci. USA* **2013**, *110*, 15931–15936.
[7] R. Walker, D. Pociecha, J. M. D. Storey, E. Gorecka, C. T. Imrie, *Eur. J. Chem.* **2019**, *25*, 13329.

[8] R. Walker, D. Pociecha, M. Salamonczyk, J. M. D. Storey, E. Gorecka, C. T. Imrie, *ChemPhysChem* **2023**, *24*, e202300106.
[9] E. Forsyth, D. A. Paterson, E. Cruickshank, G. J. Strachan, E. Gorecka, R. Walker, J. M. D. Storey, C. T. Imrie, *J. Mol. Liq.* **2020**, *320*, 114391.
[10] R. J. Mandle, *Soft Matter* **2016**, *12*, 7883.
[11] R. J. Mandle, E. J. Davis, S. A. Lobato, C. C. A. Vol, S. J. Cowling, J. W. Goodby, *Phys. Chem. Chem. Phys.* **2014**, *16*, 6907.
[12] R. Walker, *Liq. Cryst. Today* **2020**, *29*, 2.
[13] D. A. Paterson, R. Walker, J. P. Abberley, J. Forestier, W. T. A. Harrison, J. M. D. Storey, D. Pociecha, E. Gorecka, C. T. Imrie, *Liq. Cryst.* **2017**, *44*, 2060.
[14] R. B. Meyer, *Les Houches Summer School in Theoretical Physics.* Gordon and Breach, New York, **1976**.
[15] I. Dozov, *Europhys. Lett.* **2001**, *56*, 247.
[16] S. P. Sreenilayam, Y. P. Panarin, J. K. Vij, V. P. Panov, A. Lehmann, M. Poppe, M. Prehm, C. Tschierske, *Nat. Commun.* **2016**, *7*, 11369.
[17] J. K. Vij, Y. P. Panarin, S. P. Sreenilayam, M. Alaasar, C. Tschierske, *Phys. Rev. Mater.* **2019**, *3*, 045603.
[18] A. F. Alshammari, D. Pociecha, R. Walker, J. M. D. Storey, E. Gorecka, C. T. Imrie, *Soft Matter* **2022**, *18*, 4679.
[19] D. Pociecha, N. Vaupotič, M. Majewska, E. Cruickshank, R. Walker, J. M. D. Storey, C. T. Imrie, C. Wang, E. Gorecka, *Adv. Mater.* **2021**, *33*, 2103288.
[20] M. Salamończyk, N. Vaupotič, D. Pociecha, R. Walker, J. M. D. Storey, C. T. Imrie, C. Wang, C. Zhu, E. Gorecka, *Nat. Commun.* **2019**, *10*, 1922.
[21] C. T. Imrie, R. Walker, J. M. D. Storey, E. Gorecka, D. Pociecha, *Crystals* **2022**, *12*, 1245.
[22] J. P. Abberley, R. Killah, R. Walker, J. M. D. Storey, C. T. Imrie, M. Salamończyk, C. Zhu, E. Gorecka, D. Pociecha, *Nat. Commun.* **2018**, *9*, 228.
[23] R. Walker, D. Pociecha, J. M. D. Storey, E. Gorecka, C. T. Imrie, *J. Mater. Chem. C* **2021**, *9*, 5167.
[24] R. Walker, D. Pociecha, G. J. Strachan, J. M. D. Storey, E. Gorecka, C. T. Imrie, *Soft Matter* **2019**, *15*, 3188.
[25] D. A. Paterson, C. A. Crawford, D. Pociecha, R. Walker, J. M. D. Storey, E. Gorecka, C. T. Imrie, *Liq. Cryst.* **2018**, *45*, 2341.
[26] C. T. Imrie, *Liq. Cryst.* **2006**, *33*, 1449.
[27] J. L. Hogan, C. T. Imrie, G. R. Luckhurst, *Liq. Cryst.* **1988**, *3*, 645.
[28] G. S. Attard, R. W. Date, C. T. Imrie, G. R. Luckhurst, S. J. Roskilly, J. M. Seddon, L. Taylor, *Liq. Cryst.* **1994**, *16*, 529.
[29] C. Meyer, G. R. Luckhurst, I. Dozov, *J. Mater. Chem. C* **2015**, *3*, 318 .
[30] M. Ali, E. Gorecka, D. Pociecha, N. Vaupotič, *Phys. Rev. E* **2020**, *102*, 032704.
[31] D. Pociecha, C. A. Crawford, D. A. Paterson, J. M. D. Storey, C. T. Imrie, N. Vaupotič, E. Gorecka, *Phys. Rev. E* **2018**, *98*, 052706.
[32] C. T. Imrie, L. Taylor, *Liq. Cryst.* **1989**, *6*, 1.
[33] R. Dennington, T.A. Keith, J.M. Millam, *GaussView 5*, 5.
[34] C. F. Macrae, I. Sovago, S. J. Cottrell, *J Appl Crystal.* **2020**, *53*, 226.
[35] E. D. Glendening, A. E. Reed, J. E. Carpenter, J. Weinhold, *NBO*, Version 3.1.
[36] M. J. Frisch, G. W. Trucks, H. B. Schlegel, G. E. Scuseria, M. A. Robb, J. R. Cheeseman, G. Scalmani, V. Barone, B. Mennucci, G. A. Petersson, H. Nakatsuji, M. Caricato, X. Li, H. P. Hratchian, A. F. Izmaylov, J. Bloino, G. Zheng, J. L. Sonnenberg, M. Hada, M. Ehara, K. Toyota, R. Fukuda, J. Hasegawa, M. Ishida, T. Nakajima, Y. Honda, O. Kitao, H. Nakai, T. Vreven, J. A. Montgomery Jr., J. E. Peralta, F. Ogliaro, M. J. Bearpark, J. Heyd, E. N. Brothers, K. N. Kudin, V. N. Staroverov, R. Kobayashi, J. Normand, K. Raghavachari, A. P. Rendell, J. C. Burant, S. S. Iyengar, J. Tomasi, M. Cossi, N. Rega, N. J. Millam, M. Klene, J. E. Knox, J. B. Cross, V. Bakken, C. Adamo, J. Jaramillo, R. Gomperts, R. E. Stratmann, O. Yazyev, A. J. Austin, R. Cammi, C. Pomelli, J. W. Ochterski, R. L. Martin, K. Morokuma, V. G. Zakrzewski, G. A. Voth, P. Salvador, J. J. Dannenberg, S. Dapprich, A. D. Daniels, O. Farkas, J. B. Foresman, J. V. Ortiz, J. Cioslowskiand, D. J. Fox, Gaussian 09, Revision E.01, Gaussian, Inc., Wallingford CT, **2009**.
[37] A. E. Blatch, I. D. Fletcher, G. R. Luckhurst, *Liq. Cryst.* **1995**, *18*, 801.
[38] G. S. Attard, R. W. Date, C. T. Imrie, G. R. Luckhurst, S. J. Roskilly, J. M. Seddon, L. Taylor, *Liq. Cryst.* **1994**, *16*, 529.

Manuscript received: November 8, 2023
Revised manuscript received: January 17, 2024
Accepted manuscript online: January 17, 2024
Version of record online: May 9, 2024